International Journal of Materials Science and Applications
2018; 7(6): 199-208
http://www.sciencepublishinggroup.com/j/ijmsa
doi: 10.11648/j.ijmsa.20180706.11
ISSN: 2327-2635 (Print); ISSN: 2327-2643 (Online)

Influence of Milling Time on Structural and Electromagnetic Properties of Manganese Doped Cobalt Ferrite Nanoparticles

Md. Ziaul Ahsan[1, 2, *], Md. Feroz Alam Khan[2], Md. Aminul Islam[2]

[1]Department of Physics, Military Institute of Science and Technology (MIST), Dhaka, Bangladesh

[2]Department of Physics, Bangladesh University of Engineering and Technology (BUET), Dhaka, Bangladesh

Email address:
ahsanziaul@sh.mist.ac.bd (Md. Z. Ahsan), fakhan@phy.buet.ac.bd (Md. F. A. Khan)

[*]Corresponding author

To cite this article:
Md. Ziaul Ahsan, Md. Feroz Alam Khan, Md. Aminul Islam. Influence of Milling Time on Structural and Electromagnetic Properties of Manganese Doped Cobalt Ferrite Nanoparticles. *International Journal of Materials Science and Applications.* Vol. 7, No. 6, 2018, pp. 199-208. doi: 10.11648/j.ijmsa.20180706.11

Received: December 8, 2018; **Accepted**: January 5, 2019; **Published**: January 23, 2019

Abstract: This paper reports on the electromagnetic properties of manganese doped cobalt ferrite nanoparticles, synthesized via solid state reaction route using the planetary ball milling technique at different milling time (8h and 12h)in order to tune the material for applications in high frequency as well as microwave devices. The XRD patterns show the cubic spinel structure of the material. The lattice constant along with other associated structural parameters are found to increase but the particle size to decrease with the milling time. The positive value of real part of permeability is found to increase with the increase of frequency for the sample of milling time 8h. But for the sample of milling time 12h, its negative value is observed below 2 kHz and after onwards it becomes positive. This negative value of real part is the signature of diamagnetic behavior at the low frequency regime, which is assumed to originate due to the dominance of antiferromagnetic effect of Mn^{2+} ions on the B site. The diamagnetic behavior may make this material suitable to be used in electromagnetic suppression or shielding devices. The real part ε' of permittivity demonstrates the normal behavior for both the sample of milling time 8h and 12h below 2 kHz and 0.1 MHz respectively. The peaks at 8MHz for the sample of milling time 8h and at 1MHz for the sample of milling time 12h in the dispersion of its imaginary part ε" indicate the resonance condition for the respective sample at the higher frequency regime, which is assumed to be originated from the faster hoping of electrons between Fe^{2+} and Fe^{3+} in the B site. At the low frequency regime, the a.c resistivity decreases almost exponentially with the increase of frequency to a certain minimum value at 10 kHz and 1 kHz for the samples of milling time 8h and 12h respectively and after onwards it becomes almost independent of frequency. The structural correlation is analyzed with the Col-Cole plot where the single incomplete semicircle corresponds to the grain boundary resistance for 12h milled sample and double incomplete semicircles to both the grain boundary and grain resistances for 8h milled sample. Almost constant characteristic impedance implies that both the permeability and permittivity are of equal value for the sample of milling time 12h and its nearer-to-zero value of eddy current loss may make this material suitable to be used in the design of microstrip/patch antenna. However the linear variation of characteristic impedance with the frequency for the sample of milling time 8h implies the tuning effect of multilayer capacitance, which may make this sample to be integrated as tuner with the microstrip/patch antenna.

Keywords: Permittivity, Permeability, Resistivity, Characteristic Impedance, Microstrip/Patch Antenna

1. Introduction

Continual advancement in the research field of materials science is producing new and innovative materials. This is resulting in either up gradation and advancement of existing products and technologies or bringing new technologies for the development of our society and environment, directly or indirectly as explained in the literatures [1-3]. Among various

materials, nanoferrites have attracted the attention of researchers, scientists and technologists due to their wide range of applications in the field of electronics, communication, drug delivery, sensors, actuators etc. [4–8]. An extremely wide variety of total solid solution in ferrite structure enables cobalt ferrite to be strongly modified keeping the crystalline structure unchanged. This fact leads the scientists, technologists, physicists and engineers to synthesize and optimize cobalt ferrites for the possibility in diversified applications starting from electronic devices to microwave devices by doping transition and rare earth elements via solid state reaction route using different methods [4-13]. This cobalt ferrite ($CoFe_2O_4$) is of inverse spinel structure where relatively larger O^{2-} ions form cubic close pack (ccp) lattice. Its tetrahedral (A) and octahedral (B) sites, formed by the oxygen ions are occupied by metal cations (Co^{2+} and Fe^{3+}) with basic formula $(Fe^{3+})[Co^{2+}Fe^{3+}]O_4$. The doping of divalent material of ionic radii (<1 Å) in place of cobalt (Co) or iron (Fe) either in A site or B site has tuning effect on structural, magnetic and electric properties, which also leads the researchers of materials science to optimize them either in bulk or nanosized for the applications in high frequency and microwave devices during the last few decades. The materials to be used in high frequency and microwave applications require having very low electrical conductivity and dielectric loss as well as high magnetic permeability as reported in the literature [14]. The controlling of these electromagnetic parameters is a challenge to the scientists, researchers, physicists, technologists and engineers for size constraint applications such as in the design of antenna for portable and mobile communication systems [1]. Over the times, the scientists, technologists and engineers made considerable efforts towards the discovery of such materials for striking balance between the permittivity and permeability in reducing the size of antenna and enhancing proper impedance matching at high frequency range for its practical applications in space born and defense communications packages.

Substrate materials of high dielectric constant can reduce the size, but suffers from two disadvantages: (i) field remains highly concentrated in high permittivity medium and (ii) decrease in characteristic impedance of substrate material results in impedance mismatch, hence, resulting in an antenna with low efficiency. These limitations and disadvantages can be overcome by loading antenna with magneto-dielectric materials [15–17]. These are engineered materials having both dielectric and magnetic properties. The properties can be suitably tailored with proper selection of ingredients, chemicals, synthesis process and proper doping for its effective use as substrate for microstrip antenna [18, 19]. Miniaturization factor for microstrip antenna is a function of permittivity and permeability of substrate material, and is described by $n=\sqrt{\varepsilon' \times \mu'}$, which dictates to have moderate value of permeability and permittivity for significant reduction in antenna size. Ni-Zn ferrite is reported suitable for the application in low frequency range. To increase the operational frequency in the high frequency band, effects of various dopants like cobalt, aluminum, copper, barium, indium, strontium etc. had been studied [20–23].

Besides, the electromagnetic properties of materials to be used in microwave device applications mostly depend on their particle size. The planetary ball milling is a versatile and cost effective technique for synthesizing nanoparticles either by dry or wet method where in the particle size is controllable by the milling time. Keeping the above in view an endeavor is made to tune permeability and permittivity to their moderate values in achieving enhanced operational frequency band by milling time (MT). As such manganese doped cobalt ferrite nanoparticles (NPs) with composition formula $Co_{1+x}Mn_xFe_{2-x}O_4$ (x=0.125) (non-stoichiometric) have been synthesized via solid state reaction route using planetary ball milling in dry method at different milling time 8h and 12h, and reported the results in this paper, which may open up porthole in the field of high frequency and microwave device applications.

2. Experimental

The sample for the present work has been prepared by the solid state reaction route using the planetary ball milling technique in dry method. The powder of Co_2O_3, MnO_2 and Fe_2O_3 were mixed in desired proportionate (non-stoichiometric ratio) and hand milled for 2 hours before calcination. After calcination at 550^0C, again the mixer was ball milled for 8h and 12h for analyzing the effect of particle size. The composition formula of the prepared samples was $Co_{1+x}Mn_xFe_{2-x}O_4$, (Non-stoichiometric) where $x = 0.125$. The calcined powders of the representative samples were used to scaling the particle size using Field Emission Electron Microscopy (FESEM) and the Energy Dispersion Spectroscopy (EDS) spectrum used to confirm the presence of their compositional elements. Image-J software was used to estimate their average particle size. Their structural properties were investigated by the X-ray diffraction (XRD) patterns using the X-ray diffractometer. The powders were then pelletized to disc and toroid shaped samples and sintered at 750°C for 1h. The disc shaped samples were used to measure the frequency dependent permittivity, resistance (R), reactance (X) and impedance (Z), and the toroid shaped samples to measure frequency dependent permeability in a Waynekerr 6500B Impedance analyzer. Their ac resistivity (ρ_{ac}) was then calculated by the conventional formula using the geometrical parameters of each disc shaped samples. The eddy current loss was calculated for both the samples using the formula [24] as below:

$$W_{eddyloss} = \omega \mu_r \mu_0 H^2 V \sin\delta \quad (1)$$

Where, V is the volume of the toroid

$$\mu_r = \mu' \, (realpart)$$

$$\sin\delta = \frac{\mu''}{\sqrt{\mu'^2 + \mu''^2}}$$

H is the magnetic field as calculated from the flux density ($H = \frac{B}{\mu_0}$) B is the flux density as calculated from the flux ($B = \frac{\varphi}{A}$, A is the face area of the toroid) φ is the flux as calculated from ($\varphi = \frac{v}{f}$, where v is the applied voltageand f is frequency)

3. Result and Discussion

3.1. Morphological and Crystallographic Study

In order to investigate the structural correlation with the electromagnetic properties, both the FESEM micrographs and XRD patterns of the representative samples of composition $Co_{1+x}Mn_xFe_{2-x}O_4$at constant Mn content (x = 0.125) but different milling time (8h and 12h)have been taken into account, which are shown in figure1.

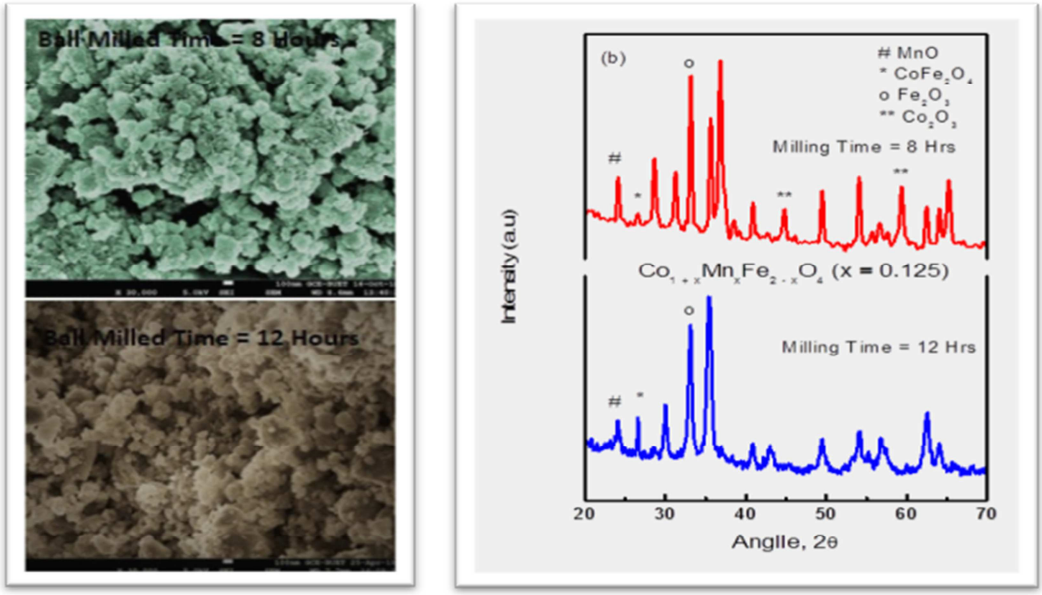

Figure 1. *(a. FESEM micrographs (b) XRD Patterns for the representative sample of the composition $Co_{1+x}Mn_xFe_{2-x}O_4$at Mn content (x = 0.125) at different milling time.*

As seen from figure 1(a), both the micrographs exhibit agglomerated and nearly spherical shaped particles. The average particle size as enumerated from the size distribution by the Image-J software is found to differ with the milling time (MT). The average particle size is found to be 19nm and 16nm for the investigated samples ball milled for 8h and 12h respectively. This variation of particle size is as usual and assumed to be within the limit of minimum possible particle size that can be obtained from the ball milling depending on milling speed and the rate of decreasing particle size. The respective EDS spectrum (not shown) confirms the presence of Co, Mn, Fe and O without any traceable amount of impurities in the composition and the estimated mass% of those constituents are listed in the table-1 as shown below:

Table 1. *Mass% and Estimated average particle size of the composition $Co_{1-x}Mn_xFe_{2-x}O_4$ at x = 0.125.*

MT	Mass %				Co:Fe	Average Particle Size (nm)
	Co	Fe	O	Mn		
8 Hours	35.76	24.62	31.52	8.10	1.452	19
12 Hours	32.76	19.56	43.14	4.54	1.675	16

From the table – 1, it is seen that the mass% of Mn content decreases with the milling time in the composition. This may have effect of reducing the average particle size due to comparatively less amount of Fe is substituted by relatively larger ionic radius of Mn in the B site of the sample of milling time 12h. Besides the mass% of Co/Fe ratio is found to increase that may have arisen from the decreased mass% of Mn in the composition and lead to disappear of the residual phase Co_2O_3, produced in the sample of milling time 8h as evident from the respective XRD patterns as shown in figure 1 (b).

Figure1 (b) shows the XRD patterns of the studied samples and the peaks as seen from these patterns confirm the crystallinity of the investigated samples. The similar pattern is observed for two samples with composition formula $Co_{1+x}Mn_xFe_{2-x}O_4$ at the same Mn content (x = 0.125) but different milling time (MT = 8 h and 12h) however their Full Width at Half Maximum (FWHM) values differ as determined by the software (match 3), which is listed in the table-2 of structural parameters. The peak at 30°, 35°, 37°, 43°, 54°, 57°and 62° corresponds to

the crystal planes (220), (311), (222), (400), (422), (511) and (400) respectively from both the XRD patterns as shown in figure 1 (b). The presence of these planes in the patterns confirms the cubic spinel structure of both samples along with residual oxide phases compared to the XRD patterns as reported in the literature [25, 26]. The highest peak is obtained at 37° for the sample of milling time 8h that corresponds to the plane (222) and used to estimate its lattice parameter. The other prominent peaks in the patterns corresponds to $CoFe_2O_4$ at 27°, 41°, 49°, corresponds to MnO at 24°, corresponds to Fe_2O_3 (hematite) at 33° and corresponds to Co_2O_3 phase at 45°, 59°that may have originated from the low calcination temperature (550°C < 800°C) to prevent the particle growth as explained in the literature [26]. On the other hand, the highest peak in the XRD patterns of the sample of milling time12h is noticed to leftward shift at angle 35°that corresponds to the plane (311) and used to estimate its lattice constant. This leftward shift of the highest peak may have originated from the disappearance of Co_2O_3 phase as observed in its XRD patterns due to increased mass% of Co/Fe ratio as mentioned above. The average crystallite size (D) of the studied samples has been estimated from the corresponding highest peaks using the Scherrer's formula [27]. The Stanley's equations [25] have been used to evaluate tetrahedral and octahedral hoping and bond lengths using the corresponding estimated lattice constants. Besides the X-ray density (ρ_x) and porosity of the studied samples have been calculated using $\rho_x = \frac{8M}{Na^3}$ [25] and $P\% = 1 - \frac{\rho_x}{\rho_b}$ [25] respectively. All the structural parameters of the studied samples are listed in the table - 2. The values of the structural parameters are almost in agreement with the literature values as reported in literature [28, 29].

Table 2. *Estimated structural parameters of the composition $Co_{1-x}Mn_xFe_{2-x}O_4$ at x = 0.125.*

MT	FWHM	D nm	*a*Å	L(A)Å	L(B)Å	(A-O)Å	(B-O)Å	ρ_xg/cm^3	P%	Stain
8 h	0.51	16.44	8.416	3.644	2.975	1.822	2.104	5.045	10.0	0.0066
12 h	0.43	19.83	8.436	3.653	2.983	1.827	2.109	5.009	8.27	0.0058

From the table-2, the lattice constant, *a*, tetrahedral hoping length L (A), octahedral hoping length L (B), tetrahedral bond length A-O, octahedral bond length B-O and crystallite size D are found to increase and the full width at half maximum (FWHM), X-ray density (ρ_xg/cm^3), porosity (P%) and strain to decrease with the milling time. The disappearance of residual phase Co_2O_3 in the composition of milling time 12h is probable reason/cause to increase *a*, L(A), L(B), A-O, B-O and D with milling time due to more homogeneity of mixing effect of solutes and dopants in the solid solution during ball milling with higher milling time (12 h > 8 h) and increased mass% of Co/Fe ratio as Co^{2+}(0.78 Å)ionic radius is greater than that of Fe^{3+}(0.49 Å) ions. However, X-ray density is found to maintain expected and usual inverse relationship with the lattice constants (*a*). Porosity is found to decrease due to increase of X-ray density and strain to decrease due to the increase of crystallite size D with the Mn content. This increased porosity may enable the sample of milling time 8h more suitable to be used in gas sensor as well.

3.2. Study on Electromagnetic Properties

3.2.1. AC Permeability

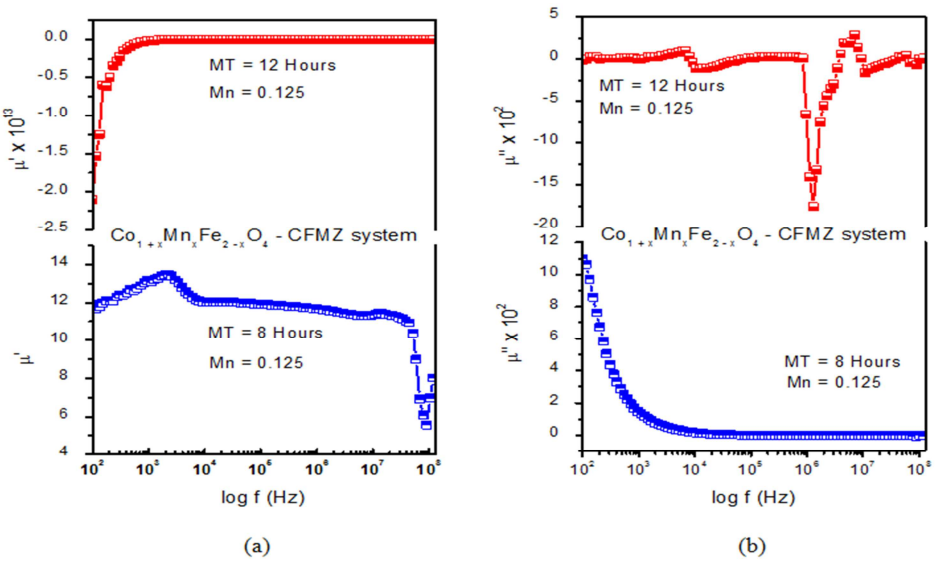

Figure 2. *(a) The real part (b) imaginary part of ac permeability as a function of frequency in logarithmic scale for the representative sample of the composition $Co_{1+x}Mn_xFe_{2-x}O_4$ at x = 0.125.*

The material having moderate and consistent value of ac permeability over wide band of frequencies is suitable for applications in high frequency and microwave devices as repotted in various literatures. This a.c permeability is a complex quantity under the influence of a.c magnetic field and is given by the relation, $\mu = \mu' - j\mu''$, where μ' corresponds to the real part that is responsible for storing magnetic energy and μ'' to imaginary part related to the dissipation of magnetic energy.Figure 2 shows the frequency response of (a) μ' and (b) μ'' for both the representative samples of milling time 8h and 12h respectively. From the figure 2(a), at low frequency regime, initially μ' is found to increase up to 2 kHz (snap shot) and to fall up to 7 MHz (snap shot) with the frequency. After onward, μ' remains almost constant with the increase of frequency and finally a sudden drop in μ' is noticed at around 44 MHz (snap shot) for the sample of 8h milling time at room temperature (RT). The permeability arises from two different magnetizing mechanisms such as spin rotation and dipolar rotation (domain wall motion), which can be described by the equation, $\mu = 1 + x_{spin} + x_{dw}$ as reported in literature [30]. Hence the initial increase of μ' up to the peak at around 2 kHz may be attributed to the combined effect of magnetic dipolar orientations (domain wall motions) and spin rotation. The decrease of μ' between 2 – 7 kHz is expected to originate from the lagging of dipolar orientation behind the applied frequency in the similar way as explained in the literature [31]. Almost constancy of μ' between 7 kHz to 44 MHz may correspond to the spin only contribution as explained in the literature [24]. However, the sudden falls of μ′ in the high frequency regime exhibits the anomalous behavior and assume to originate from the damping mechanism of spins under the influence of applied a.c magnetic field due to antiferromagnetic effect of Mn^{2+} on B site as reported in the literature [1]. Almost constant small value of μ′ is observed in the dispersion of μ′ after 2 kHz, which may originate from the spins rotation only due to smaller particle size of the samples of milling time12h as seen from the corresponding graph of figure 2 (a). However their negative value of μ′ is found to be significant below 2kHz (snapshot) in the dispersion of μ′ at the low frequency regime, which is the signature of diamagnetic behavior and expected to originate from the formation of magnetic dipoles opposite to the applied magnetic field due to the dominance of antiferromagnetic effect of Mn^{2+} ions on the B site as explained in the literature [24]. This diamagnetic behavior may make the studied material of milling time 12h suitable to be used in electromagnetic suppression or shielding devices. From figure 2 (b), it is seen almost a sharp decrease of μ″ below 2 kHz (snap shot) in its dispersion for the sample of milling time 8h. This corresponds well as μ′ rises to a maximum value around the same frequency regime as shown in figure 2(a). This behavior of μ″ assumes to originate from the damping of dipolar orientation because of lagging in frequency and finally above 2 kHz it becomes nonresponsive to the applied magnetic field as explained in the literature [26]. Contrary to this, μ″ is found to nonresponsive below 2 kHz but responsive at 1.2 MHz (snap shot) for the samples of milling time 12h, which is assumed to come out from the spin rotational resonance due to the confinement effect of smaller particle size (16nm) as explained in the literature [1].

3.2.2. AC Permittivity

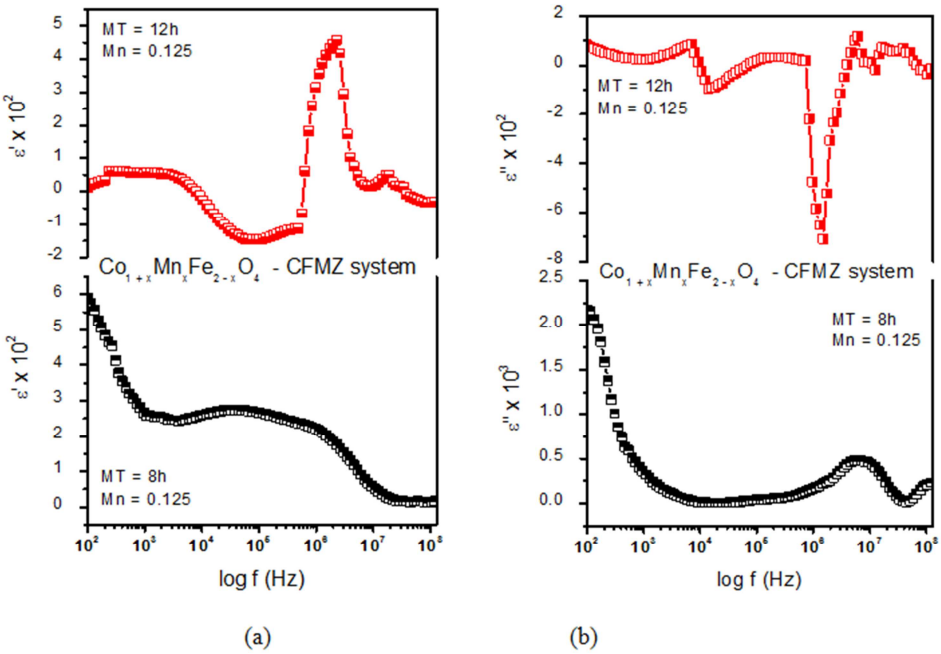

Figure 3. *(a) The real part (b) imaginary part of ac permittivity as a function of frequency in logarithmic scale for the representative sample of the composition* $Co_{1+x}Mn_xFe_{2-x}O_4$ *at x = 0.125.*

The dielectric constant or permittivity is another characteristic parameter of electromagnetic properties, which is equally important of a material to be considered for the application in high frequency and microwave devices. In the a.c field, the dielectric constant or permittivity becomes a complex quantity and is described by the relation $\varepsilon = \varepsilon' - j\,\varepsilon''$, where ε' is the real part of permittivity responsible for storing electrical energy, and ε'' is its imaginary part related to the dissipation of electrical energy in the form of heat. The permittivity is due to polarization and governed by four mechanisms such as dipole polarization, interfacial (space charge) polarization, ionic polarization and electronic polarization. The first two polarizations contribute in the low frequency band whereas the last two polarizations in the high frequency band as reported in various literatures [1, 21, 32 – 40]. Therefore the frequency response of this property depends on the frequency response of the aforesaid four mechanisms under the influence of a.c electric field. Besides the dielectric properties of ferrite materials are influenced by many factors like fabrication method, structural homogeneity, cation distribution, grain size, density, porosity, history of sintering, etc. [41, 42]. Figure 3 show the frequency response of both (a) ε' and (b) ε'' as a function of frequency in logarithmic scale for the representative samples at constant Mn content (x = 0.125) but different milling time (MT = 8h and 12h). From figure 3(a), ε' is found to exhibit the normal behavior up to 2 kHz for the sample of milling time 8h and up to 0.1 MHz for the sample of milling time 12h. This behavior can be explained on the basis of Maxwell Wagner polarization model, which suggested that both the conductivity and dielectric constant have the common origin of charge carrier and hoping between Fe^{2+} and Fe^{3+} ions in the ferrite materials as explained in the literature [43]. At lower frequencies, the hoping frequency of charge carriers follows the applied a.c field, which results in the increase of ε'. However at higher frequencies, the hoping frequency of charge carriers lag behind the applied field and hence ε'decrease due to the random dipolar orientations for both the samples of milling time 8h and 12has explained in the literature [48]. The dispersion of ε' between 2 kHz – 8 MHz and 1 – 10 MHz for the samples of milling time 8h and 12h respectively demonstrates anomalous behaviour because of the change of space charge polarization to ionic polarization due to the presence of ferrous ions in their B sites as explained in the literature [26]. Figure3 (b) shows the dispersion of ε'' for both the samples of milling time 8h and 12h. The peaks at 8 MHz for the sample of milling time 8h and at 1 MHz for the sample of milling time12h in their respective dispersion of ε'' indicates the resonance condition, which assumed to be originated from the faster hoping of electrons between Fe^{2+} and Fe^{3+} in their B site as explained in the literature [26]. However, a rightward shift of resonant peak (8MHz) for the sample of milling time 8h as compared to the peak (1MHz) of the sample of milling time 12hcan be attributed to the larger particle size, produced due to evolution of residual phase Co_2O_3 within the solubility limit of dopant and less probable mixing of constituents in the sample of milling time 8h.

3.2.3. AC Resistivity and Conductivity

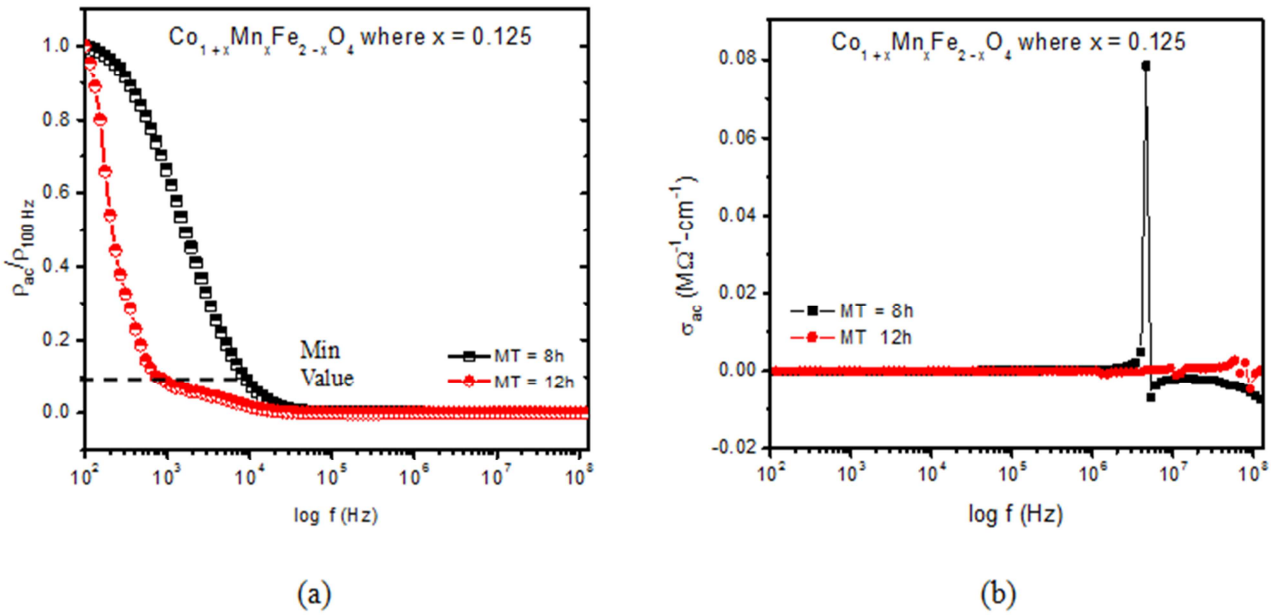

Figure 4. *(a) The normalized resistivity (b) ac conductivity $\rho_{ac}/\rho_{100\,Hz}$ as a function of frequency in logarithmic scale for the representative sample of the composition $Co_{1+x}Mn_xFe_{2-x}O_4$ at x = 0.125.*

Figure 4 show the variation of a.c resistivity and ac conductivity as a function of frequency in logarithmic scale for both the samples of milling time 8h and 12h at constant Mn content (x=0.125). Here the ratio $\left(\frac{\rho_{ac}}{\rho_{100\,Hz}}\right)$ is described as the normalized resistivity with respect to the resistivity at 100 Hz of respective sample to get the exact trend of variation for

comparison. From the figure 4 (a), it is seen that at the low frequency regime, the a.c resistivity $\left(\frac{\rho_{ac}}{\rho_{100\,Hz}}\right)$ decreases almost exponentially with the increase of frequency to a certain minimum value for the samples of milling time 8h and 12h, which differs from each other in frequency (1kHz for 12h and 10kHz for 8h), and after onwards becomes almost independent of frequency. The decrease in ρ_{ac} can be describe by the Koop's phenomenological theory, which suggests that the ferrite compact acts as multilayer capacitors and also the grain and grain boundaries have accounted for possessing different properties. The effect of multilayer capacitors increases with the increase of frequency leading to cause this decrease in ρ_{ac} as explained in the literature [44 - 47]. However, the difference in frequency at which certain minimum value of ρ_{ac} is obtained may be attributed to the relative contributions of grain boundaries to ρ_{ac} due to different particle size produced from different milling time as discussed above. From figure 4 (b) it is seen that the a.c conductivity, σ_{ac} shows the unchanged variations in the lower frequency region other than a sudden rise / fall i.e. dispersion in σ_{ac} at the higher frequency regime for both the samples of milling time8h and 12h, which is assumed to be related with the dielectric relaxation caused by the localized charge carriers across the grain boundaries and their faster response in electron hopping due to the presence of ferrous ions in their B site as explained in the literature [26]. The highest peak in the dispersion of σ_{ac} may correspond to the highest number of hoping electrons due to larger particle size.

3.2.4. Characteristic Impedance, Impedance and Eddy Current Loss

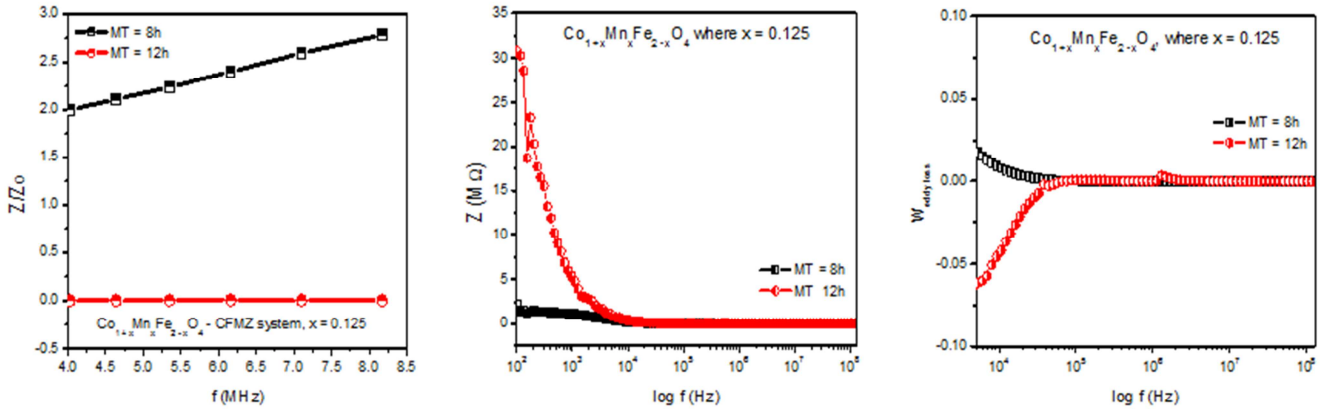

Figure 5. *(a)$\frac{Z}{Z_o}$vs log f (a) Zvs log f (c) $W_{eddy\ loss}$vs log f for the sampleof $Co_{1+x}Mn_xFe_{2-x}O_4$, at x = 0.125.*

Characteristic impedance is one of the important electromagnetic parameters to govern the proper impedance matching for maximum power transfer from the feeder line to the input of the antenna. This characteristic impedance is described by the relation,$Z = Z_o\frac{\mu'}{\varepsilon'}$ [1]. The variation of this characteristic impedance is found to be almost constant for the sample of milling time 8h but to slight linear increase for the sample of milling time 12h with the increase of frequency over 4 – 8.25MHz frequency band as shown in figure- 5(a). Almost constant characteristic impedance implies that both the permeability and permittivity are of equal value for the sample of milling time12h, which may make this material suitable to be used as substrate of the patch antenna for proper impedance matching as explained in the literature [24]. On the other hand, almost linear frequency response of this characteristics impedance for the sample of milling time 8h signifies that either μ' increase or ε'decrease with the increase of frequency. As μ' is found to remain almost constant over this frequency range as seen from figure 2(a), so ε' may decrease due to multilayer capacitance effect as discussed above of which it may make this material suitable to be used in tuning/tank circuit with the patch antenna. Fromfigure5(b), it is observed that the impedance for both the sample of milling time 8h and 12h remain almost of equal values and becomes almost independent of frequency at the high frequency region, which implies the decrease of ε' of both the samples due to effects of multilayer capacitance. The eddy current loss $W_{eddy\ loss}$ as calculated from the real and imaginary parts of permeability is to be considered in high frequency and microwave device applications and desirable to keep its value nearer to zero. Figure 6(c) shows the variation of normalized eddy current loss ($W_{eddy\ loss}$) as a function of frequency in logarithmic scale. It is seen that the eddy current loss decrease for the sample of milling time 8h whereas increase for the sample of milling time12h with frequency up to around 100 kHz and after onwards remains independent of frequency at around 0.002 value (snap shot), which make them suitable to be used in high frequency applications, in particular in the design of microstrip / patch antenna as explained in the literature [24]..

3.3. Structural Correlation

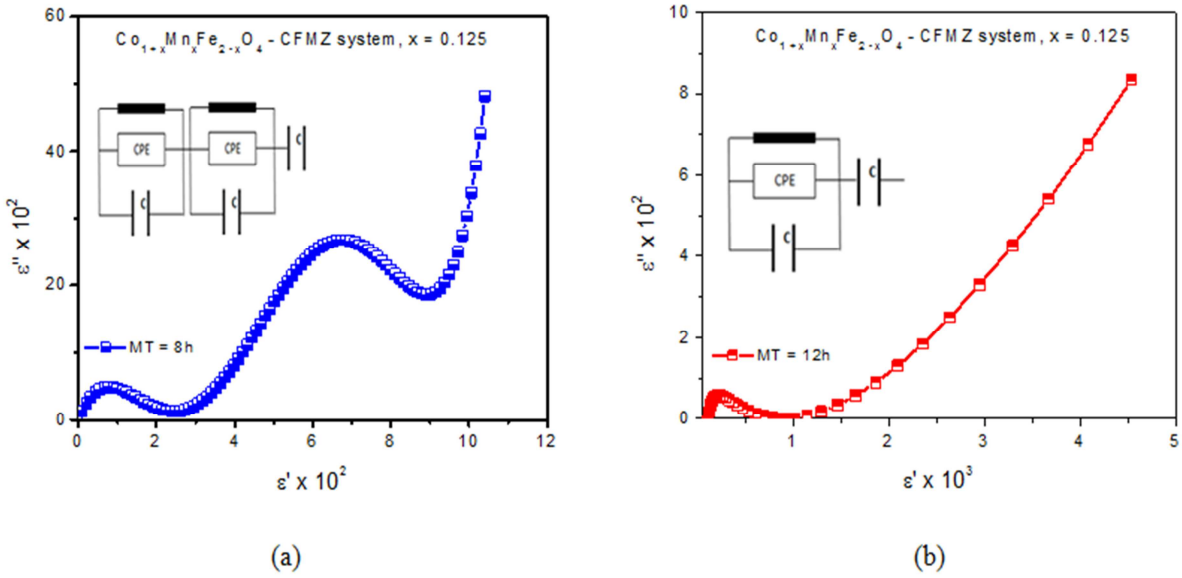

Figure 6. *(a) The Cole-Cole plot for (b) the sample of MT 8h (b) for the sample of MT 12h ofthe composition* $Co_{1+x}Mn_xFe_{2-x}O_4$ *at x = 0.125.*

In order to analyze the structural correlation with the dielectric properties, the Cole-Cole plot for the representative samples of $Co_{1+x}Mn_xFe_{2-x}O_4$ system at the same Mn content (x=0.125)but with different milling time (MT = 8h and 12h) are presented in figure6along with their equivalent circuits (inset of respective figures). In figure 6 (a) the Cole-Cole plot for the sample of milling time 8h shows the incomplete depressed two semicircles in the high frequency region. Two semicircles signify the contribution of grain boundary resistance and grain resistance with two different relaxation time of non-ideal Debye relaxation. The non-ideal Debye relaxation demands to include constant phase element (CPE) in parallel to the ideal resistor-capacitor (RC) circuit to fit the data. In the low frequency region, straight line like spikes are observed, which may be thought of another capacitance in series with the parallel combination of RC circuit. Hence, for the two semicircles as obtained from the sample of MT 8h, the Cole-Cole equivalent circuit may be assumed of the series combination of two similar parallel RC circuits and a capacitor as shown in the inset of figure 6 (a). However, as one semicircle corresponding to the grain boundary resistance, along with a straight line like spike is obtained for the sample of milling time 12h as shown in figure 6(b). As such the corresponding Cole-Cole equivalent circuit may be thought of a single similar circuit in series with a capacitor as shown in the inset of figure 6 (b). The appearance of double semicircles may have originated from the larger number of gain boundaries due to its larger particle size for the sample of milling time 8h as evident from the table-1.

4. Conclusion

Nanoparticles of manganese doped cobalt ferrite with non-stoichiometric composition $Co_{1+x}Mn_xO_4$ for x = 0.125 have been synthesized via solid state reaction route using ball mill technique at different milling time 8h and 12h. The existence of peaks in the XRD patterns for them confirms the crystallinity and cubic spinel structure as well. The highest peak for the sample of milling time 8h shifts rightward and implies the decrease in lattice constant compared to that of the sample of milling time12h due to increase of particle size. The sample of 8h milling time shows an increment of μ' up to 2 kHz and decrement up to 7 MHz with the frequency. After onward μ' remains almost constant due to spin only contribution. Finally a sudden drop in μ'at 44 MHz is noticed and demonstrates anomalous frequency response due to the damping mechanism of spins originated from the antiferromagnetic effect of Mn^{2+} on the B site. On the other hand the negative value in μ' of the sample of 12h milling time is significant below 2 kHz and exhibits diamagnetic behavior due to the formation of magnetic dipoles opposite to the applied field, which make it suitable to be used in electromagnetic suppression or shielding devices. The behavior of μ'' is responsive to the applied frequency below 2 kHz but afterwards nonresponsive for the sample of 8h whereas it is nonresponsive below 2 kHz but responsive after onwards for the sample of 12h milling time due to spin rotational resonance for relatively smaller particle size. The dispersion in ε' between 2 kHz – 8 MHz and 1 – 10 MHz for the samples of milling time 8h and 12h respectively demonstrates anomalous behaviour due to change of space charge polarization to ionic polarization for the presence of ferrous ions in the B sites. The peaks at 8 MHz for the sample of milling time 8h and at 1 MHz for the sample of 12h in the dispersion of ε'' indicates the resonance condition and assumed to be originated from the faster hoping of electrons between Fe^{2+} and Fe^{3+} in the B site. However, a rightward shift of resonant peak (8MHz) for the sample of milling time 8h as compared to the peak (1MHz) of the

sample 12hcan be attributed to the larger particle size, produced due to evolution of additional residual phase Co_2O_3 within the solubility limit of dopant and less probable mixing of constituents in the sample of milling time 8h. In the lower frequency regime, ρ_{ac} decreases almost exponentially with the increase of frequency to a certain minimum values at 1kHzand 10 kHz for the samples of 12h and 8h respectively due to increase of multilayer capacitance. The incomplete depressed two semicircles for the sample of 8h and one semicircle for the sample of 12h are observed in the Cole-Cole plot respectively to show structural correlation with the electrical properties. The double semicircles corresponds to grain boundary and grains resistances and single semicircle to the grain boundary resistance to the a.c dielectric constant as well resistivity of the samples of 8h and 12h respectively. The characteristic impedance is the governing factor for impedance matching, which is constant for the sample of 12h whereas slight linear increase is noticed for the sample of 8h over 4 – 8.25 MHz frequency band. The constancy in characteristic impedance signifies here the equality in μ' and ε' for the sample of 12h but the slight increase corresponds to decrease in $\varepsilon'$for the sample of 8h with the increase of frequency. Besides, both the samples show almost zero eddy current loss ($W_{eddy\ loss}$) after 100 kHz. Hence, the constancy in characteristic impedance and almost zero eddy current loss make the sample of 12h suitable to be used in microstrip/patch antenna design and the variation of characteristic impedance over the frequency band 4 - 8.25 MHz may make the sample of 8h suitable for tuner circuit along with the microstrip/patch antenna. However further investigations are suggested on its conjugate non-stoichiometric composition $Co_{1-x}Mn_xFe_{2+x}O_4$ ($0 \leq x \leq 0.5$) aiming at its applicability in high frequency and sensor devices.

Acknowledgements

The authors are thankful to the International Science Programs (ISP), Uppsala University, Sweden for financial and technical support. The authors are also thankful to the Department of Glass and Ceramics Engineering (GCE), Bangladesh University of Engineering and Technology (BUET), and to the Department of Physics, Military Institute of Science and Technology (MIST) for their experimental support.

References

[1] A. Saini, P. Kumar, B. Ravelo, S. Lallechere, A. Thakur, P. Thakur. Magneto-dielectric properties of doped ferrite based nanosized ceramics over very high frequency range. *Engineering Science and Technology an International Journal, 19(2016) 911-916.*

[2] R. B. Nikodem, New generation solar control coated products. *J. Vac. Sci. Technol. A. 10 (1992) 1884–1891.*

[3] J. E. Hilland, F. V. Stuhr, A. Freeman, D. Imel, Y. Shen, R. L. Jordan, et al. Future NASA space borne SAR missions. *IEEE Aerosp. Electron Syst. Mag. 13 (1998) 9–16.*

[4] S. E. Lyshevski. Nano-, NanoBio- and NanoBio Medical-Technologies: Enabling sensing, communication and processing paradigms. *12th IEEEConference on Nanotechnology, (2012)1-2.*

[5] K. M. Krishnan. Biomedical nanomagnetics: a spin through possibilities in imaging, diagnostics, and therapy. *IEEE Trans. Magn, 46(2010), pp. 2523-2558.*

[6] M. F. L. De Volder, S. H. Tawfick, R. H. Baughman, A. J. Hart. Carbon nanotubes: present and future commercial applications. *Science 339 (2013) 535–539.*

[7] T. L. Chang, Y. W. Lee. Applications of magnetic nanoparticles in engineering and biomedical science. *7th IEEE Conference on Nanotechnology (2007) 656–659.*

[8] S. E. Lyshevski, K. S. Martirosyan. Ferrite nanoparticles for MEMS technology sensors and actuators. *11th IEEE Conference on Nanotechnology (2011) 1252– 1256.*

[9] S. Bhattacharya, S. Maity, S. K. Metya, C. T. Bhunia, Performance enhancement of implantable medical antenna using differential feed technique. *Eng. Sci. Technol. Int. J. (2015) doi:10.1016/j.jestch.2015.09.001 In press.*

[10] I. Bibyk, R. Romanofsky, E. Wintucky. RF technologies for advancing space communication infrastructure. *IEEE Aero Conference (2006).*

[11] D. A. Grier. The innovation curve [Moore's law in semiconductor industry]. *Computer 39 (2006) 8–10.*

[12] R. R. Schaller. Moore's law: past, present and future. *IEEE Spectrum. 34 (1997) 52–59.*

[13] R. Bala, A. Marwaha. Investigation of graphene based miniaturized tetra hertz antenna for novel substrate materials. *Eng. Sci. Technol. Int. J. (2015)doi:10.1016, j.jestch.2015.08.004 In press.*

[14] R. Ahmad, I. Hussain Gul, M. Zarrar, Humaira Anwar. Improved electrical properties of Cd substituted cobalt ferrite nanoparticles for microwave application. *Journal of magnetism and magnetic materials, 405(2016)28-35.*

[15] R. C. Hansen, M. Burke. Antennas with magneto-dielectrics. *Microw. Opt. Techno. Lett. 26 (2000) 75–78.*

[16] H. Mosallaei, K. Sarabandi. Magneto-dielectrics in electromagnetics: concept and applications. *IEEE Trans. Antennas Propag. 52 (2004) 1558–1567.*

[17] K. Min, T. Hong. Miniaturization of antenna using magneto-dielectric materials. *IEEE Asia-Pacific Conf. Commun. (2006)1–5.*

[18] P. Mathur, A. Thakur, M. Singh. A study of nanostructured Zn-Mn soft spinel ferrites by citrate precursor method. *Phys. Scripta. 77 (2008) 045701*

[19] S. Chaimool, A. Pinsakul, P. Akkarae kthalin, Patch antenna miniaturization using artificial magneto-dielectric met substrate. *International Symposium on Antennas and Propagation (2012)906–909.*

[20] K. Rana, P. Thakur, P. Sharma, M. Tomar, V. Gupta. Improved structural and magnetic properties of cobalt nanoferrites: influence of sintering temperature. *Ceramic Int. 41 (2015) 4492–4497.*

[21] P. Mathur, A. Thakur, M. Singh. Low temperature synthesis of $Mn_{0.4}Zn_{0.6}In_{0.5}Fe_{1.5}O_4$ nanoferrites for high frequency applications. *J. Phys. Chem. Solids 69 (2008) 187–192*.

[22] L. B. Kong, M. L. S. Teo, Z. W. Li, G. Q. Lin, Y. B. Gan. Development of magneto-dielectric materials based on Li-ferrite ceramics. *J. Alloy. Compd. 459 (2008) 576–582.*

[23] A. Saini, A. Thakur, P. Thakur, Matching permeability and permittivity of $Ni_{0.5}Zn_{0.3}Co_{0.2}In_{0.1}Fe_{1.9}O_4$ ferrite for substrate of large bandwidth miniaturized antenna. *J. Mater. Sci. (2015)doi:10.1007/s10854-015-4095-8 In press.*

[24] M. Z. Ahsan, F. A. Khan, M. A. Islam, T. Tabassum, M. K. Alam. Study on AC permeability and permittivity of manganese doped cobalt ferrite nanoparticles. *J. Phys. Commun. 2 (2018) 105008:1 – 6.*

[25] M. Z. Ahsan, F. A. Khan. Study of Structural, Electrical and Magnetic Properties of Manganese Doped Cobalt Ferrite Nanoparticles with Non-stoichiometric Composition. *Journal of Physical Science and Application (2017) 7(6):30-7.*

[26] M. Z. Ahsan, F. A. Khan. Structural and electrical properties of manganese doped cobalt ferrite nanoparticles. *Mater Sci. Nanotechnol. (2018)2(2):1-9.*

[27] S. P. Yadav, S. S. Shinde, A. A. Kadam. Structural, morphological, dielectric and magnetic properties of Mn substituted cobalt ferrite. *Journal of Semiconductor, . (2013)," 34:093002.*

[28] N. Ponpandian, P. Balaya, A. Narayanasamy. Electrical conductivity and dielectric behaviour of nanocrystalline $NiFe_2O_4$ spinel. *Journal of Physics: Condensed Matter (2002) 14: 3221.*

[29] M. Z. Ahsan, F. A. Khan. Study on Effects of Mn Substitution in Cobalt Ferrite. *International Conference on Mechanical Engineering and Applied Science (ICMEAS) 2017, Military Institute of Science and Engineering, Dhaka-1216.*

[30] P. Mathur, A. Thakur, M. Singh. Study of low temperature sintered nanocrystalline Mn-Cu-Zn ferrite prepared by co-precipitation method. *Mod Phys. Lett. B 21 (2007) 1425–1430.*

[31] S. Bawawaje, M. Hashi, I. Ismail. Effects of Sintering Temperature on the Grain Growth and Complex Permeability of $Co_{0.2}Ni_{0.3}Zn_{0.5}Fe_2O_4$ material prepared using mechanically alloyed nanoparticles. *Journal of Magnetism and Magnetic Materials 323(2011) 1433-9*.

[32] K. Rana, P. Thakur, P. Sharma, M. Tomar, V. Gupta., Improved structural and magnetic properties of cobalt nanoferrites: influence of sintering temperature. *Ceramic Int. 41 (2015) 4492–4497*.

[33] L. B. Kong, M. L. S. Teo, Z. W. Li, G. Q. Lin, Y. B. Gan. Development of magneto-dielectric materials based on Li-ferrite ceramics. *J. Alloy. Compd. 459 (2008) 576–582.*

[34] A. Thakur, P. Thakur, J.-H. Hsu. Enhancement in dielectric and magnetic properties of In3+ substituted Ni-Zn nanoferrites by co-precipitation method. *IEEE Trans. Magn. 47 (2011) 4336–4339.*

[35] A. Thakur, P. Mathur, M. Singh. Processing of nanocrystalline spinel ferrite prepared by co-precipitation method. *Int. J. Mod. Phys. B 23 (2009) 365–374*.

[36] A. Thakur, A. Chevalier, J.-L. Mattei, P. Queffélec. Suitability of Ni-Zn ferrites ceramics with controlled porosity as granular substrates for mobile handset miniaturized antennas. *IEEE Trans. Magn. 47 (2011) 3720–3723.*

[37] A. Pathania, P. Thakur, A. Sharma, J. H. Hsu, A. Thakur. Investigation of iron deficient and manganese doped Ni-Mg nano-ferroxide ceramics. *Ceramic Int. 41 (2015) (2015) 10803–10809.*

[38] A. Thakur, P. Mathur, M. Singh. Controlling the properties of Mn-Zn ferrites at high frequency by substituting In3+ and Al3+ ions. *Ind. J. Pure Appl. Phys. 46 (2008) 47–53.*

[39] P. Mathur, A. Thakur, M. Singh. Effect of nanoparticles on the magnetic properties of Mn-Zn soft ferrite. *J. Magn. Magn. Mater. 320 (2008) 1364–1369*.

[40] P. Mathur, A. Thakur, J. H. Lee, M. Singh. Sustained electromagnetic properties of Ni-Zn-Co nanoferrites for the high frequency applications. *Mater. Lett. 64 (2010) 2738–2741.*

[41] R. Nongjai, S. Khan, K. Asokan. Magnetic and electrical properties of In doped cobalt ferrite nanoparticles. *J Appl Phys. 2012; 112:084321.*

[42] S. E. Shirsath, B. G. Toksha, K. M. Jadhav. Structural and magnetic properties of In3+ substituted $NiFe_2O_4$. *Mater Chem Phys. 2009; 117:163*.

[43] R. C. Kambale, P. A. Shaikh, C. H. Bhosale. The effect of Mn substitution on the magnetic and dielectric properties of cobalt ferrite synthesized by an auto combustion route. *Smart Mater Struct. 2009; 18:115028.*

[44] N. Rezlescu, E. Rezlescu. Dielectric properties of copper containing ferrites. *Phys Status Solidi A. 1974;23(2):575.*

[45] C. G. Koop's. On the dispersion of resistivity and dielectric constant of some semiconductors at audio frequencies. *Phys Rev. 1951; 83(1):121–4*.

[46] A. Thakur, P. Thakur, J. H. Hsu, "Magnetic behaviourof$Ni_{0.4}Zn_{0.6}Co_{0.1}Fe_{1.9}O_4$ spinel nanoferrite. *J. Appl. Phys. 111 (2012) 078305.*

[47] S. S. Thakur, A. Pathania, P. Thakur, A. Thakur, J. H. Hsu, Improved structural, electrical and magnetic properties of Mn–Zn–Cd nanoferrites. *Ceramic. Int. 41 (2015) 5072–5078*.